UC-34C
LBL-6558
Preprint C.1

Submitted to Physical Review C

ENERGY SPECTRA OF NUCLEAR FRAGMENTS PRODUCED BY HIGH ENERGY PROTONS

G. D. Westfall, R. G. Sextro, A. M. Poskanzer,
A. M. Zebelman, G. W. Butler, and E. K. Hyde

December 1977

Prepared for the U. S. Department of Energy
under Contract W-7405-ENG-48

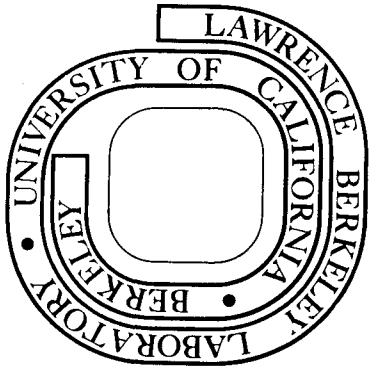

DISCLAIMER

for Phys Rev C
Index 25.40.Rb
14 Dec 77

LBL-6558

ENERGY SPECTRA OF NUCLEAR FRAGMENTS PRODUCED BY HIGH ENERGY PROTONS

G. D. Westfall, R. G. Sextro, A. M. Poskanzer, A. M. Zebelman,* G. W. Butler,† and E. K. Hyde

Lawrence Berkeley Laboratory
Berkeley, California 94720

ABSTRACT

Fragment energy spectra from the 2.1- and 4.9-GeV proton irradiation of C, Al, Ag, and U targets were measured at several angles to the beam for products ranging from He up to Ar for the heavier targets. The fragments were detected in a telescope consisting of a gas ΔE counter and a silicon E counter. The carbon target measurements are compared with previous data from projectile fragmentation studies. A Maxwellian type functional form which fits the energy spectra from all the targets is presented. The spectra were integrated to obtain values of the cross section as a function of atomic number.

NUCLEAR REACTIONS C(p,X), E = 2.1, 4.9 GeV; measured $\sigma(E,\theta)$, X = He to C. Al(p,X), E = 2.1, 4.9 GeV; measured $\sigma(E,\theta)$, X = He to Na. Ag(p,X), E = 4.9 GeV; measured $\sigma(E,90°)$, X = N to Ar. U(p,X), E = 4.9 GeV; measured $\sigma(E,\theta)$, $\sigma(X)$, X = F to Ar. Spallation, fragmentation.

I. INTRODUCTION

Reactions of high energy protons with complex nuclei are not fully understood. Some of the most revealing information about such reactions has come from the study of the energy spectra of emitted fragments. In this paper improved experimental technique has allowed the extension of measurements to lower kinetic energies and to heavier fragments. Our previous studies of the energy spectra of fragments produced from silver,[1,2] and uranium[2,3] targets by 5 GeV protons were limited by a low energy cut off in the measurements because of the thickness of the silicon ΔE detectors used in the telescopes. This cut off ranged from about 1.5 MeV/nucleon for the lighter fragments up to 3 MeV/nucleon for Ar fragments, and prevented the observation of the "evaporation" peak in the energy spectra for these heavier fragments from silver and uranium targets. Since it was difficult to obtain thinner silicon detectors with the required uniformity, the present study used a gaseous ionization chamber for the ΔE detector, thus allowing measurements down to 0.6 MeV/nucleon for all fragments. Because the gas telescope only resolves elements in this energy range, the original plan was to combine it with a time of flight measurement[4] to obtain both element and isotope resolution. Even though the plan has not been realized, this new low energy cut off with only Z resolution made it interesting to also make measurements of spallation residues from light targets such as carbon and aluminum. In particular the reaction of 2.1 GeV protons on a carbon target was studied to compare with the same reaction of 2.1 GeV/nucleon carbon ions on a hydrogen target, which has been studied by the technique of projectile fragmentation.[5] The rather complete data from the aluminum target should allow comparison

with theory, such as cascade-evaporation calculations. Both sets of data should be of astrophysical interest. The fragments from the heavier targets are of interest in understanding the statistical break up of highly excited nuclei.

In addition a functional form is presented which fits the energy spectra from all four targets. The parameters of these fits are presented and they are used in some cases to help integrate the energy spectra to obtain cross sections. The physical significance of the parameters is discussed.

Energy spectra of fragments from reactions induced by high energy protons have been studied by many techniques in the past. From a carbon target ^{8}Li has been measured with nuclear emulsions,[6,7] and ^{11}C by activation techniques.[8] Thick target recoil techniques have also been used[9,10] for ^{11}C. Counter telescope experiments using the ΔE-E technique are summarized[11] in Table I. (See also Ref. 12). At lower incident energies time of flight techniques have been used.[13,14] Studies have also been done on a boron target using counters[15] and an oxygen target using emulsions.[16] From an aluminum target ^{8}Li has also been studied[6,7] and counter telescope experiments have also been performed.[11,12] The production of ^{24}Na from aluminum has been extensively studied by radioactive recoil techniques.[17-21] Surveys of the literature for the silver and uranium targets are contained in Refs. 1 and 3, respectively. More recent counter telescope experiments are summarized[22-26] in Table I. Thin target[27-29] (Cl, V, Cu, Ag, Bi) and thick target[30] (Au, U) radiochemical recoil measurements have been performed for ^{24}Na.

II. EXPERIMENTAL

The experiments were done at two different times. The measurements for the aluminum target with silicon detectors were performed at the same time as the previously published Ag and U data,[1,3] and the details for these experiments have already been described.[3] The silicon telescope measurements for the carbon target are more recent but were done in the same way. All the silicon telescopes used are described in Table II. The measurements with the gas ionization chamber will be described here in more detail.

The gas telescope, which consisted of a gas ΔE counter and a silicon E counter, was a copy of the one developed by Fowler and Jared.[31] It consisted of a Frisch grid ionization chamber as the ΔE detector with the silicon E detector placed inside the gas counter assembly. The main difference was that the entrance window was enlarged to be 8 mm in diameter. The window consisted of five laminations of Formvar with a total thickness of 50 $\mu g/cm^2$ supported by four crossed 0.025 mm stainless steel wires in a square array. The calculated transmission was 98.6%. The distance between the window and the E detector was 7.1 cm. The counter gas was argon with 7% methane at a pressure of 50 torr. The resulting thickness of the ΔE counter was 0.76 mg/cm^2, equivalent to about 3 μm of silicon. The gas flow was about 0.6 torr-liters/sec. The pressure was stabilized to $\pm 1\%$ by a Cartesian manostat and read remotely by a pressure transducer connected to a digital voltmeter. The ionization chamber anode plate was operated at +350 volts, and the grid at +80 volts. At this pressure the plate voltage plateau was at least 200 volts wide and the grid voltage had considerable leeway on

either side of its value. The energy calibration was obtained using a pulser and a reference capacitor whose value was calculated assuming 26.1 ev/ion-pair[32] for this argon-methane mixture. The calibration was accurately checked by raising the pressure to stop 6 MeV alpha particles in the gas.

The first stage of the ΔE preamplifier was mounted inside the gas counter, directly coupled to the anode. The capacitance of the ion chamber was measured to be 10-15 pF, including the field effect transistor of the preamp. The electronic resolution measured with a pulser was about 17 KeV full width at half maximum (FWHM). For alpha particles the resolution (after root-mean-square subtraction of the electronic resolution) was 9-12% FWHM for energies deposited in the counter from 450 to 150 keV.

The E detector was a nominal 100 μm partially depleted silicon surface barrier detector, 100 mm^2 in area. The electronic coincidence time resolution between the silicon and the anode was 23 ns FWHM. Since the electron collection in the gas was perpendicular to the path of the fragments, the collection time depended upon the distance between the particle path and the anode plate. Thus the time resolution for real particles depended on the size of the entrance window, being 75 ns FWHM for a 2 mm diameter window and 160 ns FWHM with the normally-used 8 mm diameter window, in agreement with calculations of electron drift times. In the future it probably would be better to use pure methane gas because of its faster electron drift velocity.

A slow coincidence was made between the ΔE and E single-channel-analyzer signals. These signals also started and stopped a time-to-amplitude converter whose output was recorded event by event so that

a tight time resolution and correction for accidentals could be obtained in the off-line analysis. The lower level of the E detector single channel analyzer was set at 1 MeV for the carbon and aluminum targets, 4 MeV for the silver target, and 5 MeV for the uranium target. A pile-up rejector was also used on the E detector. A plot of ΔE vs E for the aluminum target data is shown in Fig. 1a. The maxima in ΔE of the ridge lines for the low energy heavier fragments is caused by the neutralization of the ions as they slow down. An analogue particle identifier (PI) was available on line, and as seen in Fig. 1b, all the elements were clearly resolved. In addition, the isotope ^{7}Be could be resolved from the other Be isotopes. The final analysis was done event-by-event with the digital PI algorithm used previously.[33] The constants of the algorithm were adjusted for groups of about six elements at a time.

The targets were oriented so that a perpendicular to their surface was at 55° with respect to the beam. The carbon target was a polystyrene film, 70 $\mu g/cm^2$ thick for the gas telescope and 410 $\mu g/cm^2$ thick for the silicon telescope measurement. The aluminum target was a sheet of hammered aluminum 170 $\mu g/cm^2$ for the gas telescope measurements. X-ray fluorescence showed the impurities in these targets to be mainly Fe, Cu, and Zn. However,the total impurities were less than 0.2% for the polystyrene and 0.6% for the hammered aluminum, and are not thought to have affected the data. For silicon telescope measurements high purity foil was used. The silver target was an evaporated film 530 $\mu g/cm^2$ thick mounted over a hole in a 0.0006 cm thick Mylar foil. The uranium target was 720 $\mu g/cm^2$ of UF_4 vaporized onto a 0.0006 cm thick Mylar backing. Products lighter than F were not recorded for the UF_4 target.

In order to obtain better statistics at 90°, the gas telescope was positioned only 12 cm from the target; these data were later renormalized to the 90° data taken at the distance of 29 cm used to obtain the angular distributions. The gas telescope data were normalized to the silicon telescope data at each angle. The absolute normalizations were done in different ways. For the carbon target data at 2.1 GeV the 90° ^{7}Be particle spectrum was matched to the data of Greiner et al,[5] and then both sets of data were renormalized so that the integrated ^{7}Be cross section was equal to the radiochemically measured value of 10.0 mb.[34,35] At 4.9 GeV the ^{7}Be from carbon cross section is 9.4 mb[34,35] and the data were reduced by the ratio 9.4/10.0 assuming that the unmeasured low-energy part of the spectrum has the same shape. For the aluminum target data the integrated ^{7}Be cross section was normalized to 8.4 mb[34,36] at both energies. These radiochemical cross sections are probably accurate to ±10%. For the silver and uranium targets the Na data were normalized to our previous results.[1-3]

III. RESULTS

Fragment energy spectra at 90° in the laboratory for carbon irradiated by 2.1 GeV protons are shown in Fig. 2. The data obtained with 4.9 GeV protons are exactly superimposeable, both with respect to shape and relative yields of the different products. In one of the replicate measurements the telescope angle must have been accidentally set at slightly less than 90° and the C spectrum showed a large increase at low energies due, surprisingly, to ^{12}C elastic recoils;[37] the data were disregarded. The ^{7}Be energy spectra at three angles to the beam are shown in Fig. 3 as an example. At 4.9 GeV, data were obtained at five angles. The activation measurements for ^{11}C which have been done[8] cover energies only up to 3 MeV which is below the range of our present data.

The 90° energy spectra of fragments from an aluminum target irradiated by 4.9 GeV protons are shown in Figs. 4 and 5. In Fig. 4 individual isotopes obtained with the silicon telescope are shown with extensions to lower energies for ^{4}He and ^{7}Be obtained by the gas telescope. In Fig. 5 the gas telescope data, which only had element resolution except for ^{4}He and ^{7}Be, are shown together with extensions to higher energies with data from the silicon telescope. Energy spectra at five angles are shown in Figs. 6 and 7 for p, He, Li, and Na products. The data at 2.1 GeV are extremely similar but were only obtained at three angles.

Moskaleva[21] has reported observing very high energy ^{24}Na fragments in the forward hemisphere from thick target recoil experiments of Al irradiated by 660 MeV protons. The reported energy spectrum drops only

a factor of ten from the peak out to 70 MeV. This is clearly inconsistent with the data in Fig. 7 as well as the previous thin target recoil experiments.[17]

The 90° energy spectra for fragments from silver are shown in Fig. 8. For this target data were only collected at 90°. Although the data extend to considerably lower energies than our previous work,[1,2] the peaks in the spectra can only be seen for products up through Ne. Surprisingly, it does not appear that the peaks are moving to higher energy with increasing Z of the fragment; this will be discussed further below. The ^{24}Na radiochemical measurements[28] appear to peak at about 17 MeV, which is somewhat lower than the Na data in Fig. 8 would indicate.

The 90° energy spectra from uranium are shown in Fig. 9. The peaks are clearly defined all the way through Ar, although the energy cut-off was not as low here because of interference from fission fragments. As an example, energy spectra for Na at three angles are shown in Fig. 10. The Na energy spectra obtained with 28 GeV incident protons[25] exhibit more filling in at low energies making the peaks less clearly defined.

IV. FUNCTIONAL FORM

It is desirable to fit the large amount of graphical data to a simple functional form with a relatively small number of parameters. Hopefully, these parameters will have some physical significance. Also, it is then easier to extrapolate to the unmeasured parts of the energy spectra for the purpose of obtaining integrated cross sections. Traditionally, the energy spectra of fragments emitted in the bombardment of medium and high mass target nuclei by high energy protons have been fit using the functional form[3]

$$P(\varepsilon) = \int_{k = <k> - \Delta}^{k = <k> + \Delta} (\varepsilon - kB) e^{-(\varepsilon - kB)/\tau} dk \quad (\varepsilon > kB) \qquad (1)$$

where ε is the fragment kinetic energy in the system of the struck nucleus, B is the coulomb barrier between the fragment and the residual nucleus, $<k>$ is the nominal barrier fraction, Δ is the smearing parameter, and τ is the temperature.

The preexponential factor, ε-kB, actually arises from the product of a Coulomb barrier penetration factor, 1-kB/ε, times the ε of the expression $\varepsilon \exp(-\varepsilon/\tau)$. The kB in the exponent is for normalization. Parameters of this equation which have been fit to data have been reported by several authors.[1,3,24,38]

A slightly different functional form is proposed here using Maxwell-Boltzman distributions involving the square root of the energy instead of the first power in the preexponential factor in direct analogy

to the available projectile fragmentation data[5] and to thermodynamic models such as the nuclear fireball model.[38] This functional form, with properly adjusted parameters, reproduces the shapes of the energy spectra of fragments from the targets considered here, and will be derived and described in detail below.

Greiner, et al.[5] have studied the projectile fragmentation of 2.1 GeV/nucleon ^{12}C ions on various targets. By studying both C and CH targets they extracted the cross sections for a hydrogen target. These results have been presented as distributions in momentum parallel to the beam direction, $p_{\parallel}$, in the projectile rest frame. The projectile fragmentation data for $C + p \rightarrow {}^{7}Be$ are shown in Fig. 11 along with the Gaussian fit to the data reported by Greiner et al.[5] This Gaussian momentum distribution is expressed as

$$\frac{d\sigma}{dp_{\parallel}} = \frac{\sigma_o}{(2\pi)^{\frac{1}{2}}\sigma_{p_{\parallel}}} e^{-(p_{\parallel} - \langle p_{\parallel} \rangle)^2/(2\sigma_{p_{\parallel}}^2)} \qquad (2)$$

where σ_o is the cross section, $\sigma_{p_{\parallel}}$ is the standard deviation or width, and $\langle p_{\parallel} \rangle$ is the displacement from the projectile momentum. If the perpendicular momentum distribution is also Gaussian with the same width, as is consistent with the data of Greiner et al.,[5] the corresponding kinetic energy (E) distribution in the ^{12}C rest frame is

$$\frac{d^2\sigma}{dE\ d\Omega} = \frac{\sigma_o}{2}\left(\frac{\pi\sigma_{p_\parallel}^2}{m}\right)^{-3/2} \sqrt{E}\ e^{-m(E+E_c-2\sqrt{EE_c}\cos\theta)/\sigma_{p_\parallel}^2} \qquad (3)$$

$$E_c = \langle p_\parallel \rangle^2/(2m)$$

where θ is the angle in the ^{12}C frame and c has been taken equal to one. In this form, the equation is immediately recognized as a Maxwell-Boltzman distribution moving relative to the ^{12}C frame. The interaction of two bodies must be the same when the roles of target and projectile are reversed, as long as the relative velocity of the two bodies remains the same. Thus when ^{12}C is the target the above equations must apply to the laboratory frame.

Using the parameters given in Ref. 5 for 2.1 GeV/nucleon ^{12}C on hydrogen, our data for 2.1 GeV p + ^{12}C can be compared directly to the projectile fragmentation results. Since our data only have element resolution, the results of eq. (3) are summed using the measured cross sections[39] for the various isotopes of a given element. In Fig. 2, the measured data for fragments at 90° in the laboratory from ^{12}C irradiated by 2.1 GeV protons are compared with the projectile fragmentation data as above. A similar comparison is made for ^{7}Be fragments at 20°, 90°, and 160° in the lab in Fig. 3. In both cases, there seems to be a low energy component corresponding to the measured projectile fragmentation results on which is superimposed a high energy tail.

Such an effect has also been seen in emulsion data.[40] Since the projectile fragmentation is represented by a Maxwell-Boltzman distribution, it seems that the data can be represented by the sum of two Maxwell-Boltzman distributions.

The data for fragments from Al also demonstrate this two component structure. However, the data for fragments from Ag and U show further characteristics. A very noticeable Coulomb barrier peak is evident, and as found previously,[3] a large amount of smearing is evident in the spectral shape. In addition, the Coulomb barrier peak of the heavier fragments from Ag seems to stop increasing with nuclear charge of the fragment in contrast to the case for fragments from U. This is probably because the mass of the fragment is becoming comparable to the mass of the recoiling residue which carries off significant amounts of the kinetic energy. Thus the kinematics of a two body breakup is indicated. This is reasonable for the heavy targets where there is likely to be a heavy residue and was included[3] in the application of equation 1 but had little effect for the cases previously studied. For the light mass targets break up into several fragments with comparable mass should be common. However the highest energies are most likely to come from the two body break ups and the lower kinetic energy fragments are not so sensitive to the kinematics.

A functional form is proposed incorporating the following features:

1. Sum of two different Maxwell-Boltzman distributions.
2. Two body break up kinematics.

3. Inclusion of a Coulomb barrier and smearing.

4. Proper normalization to allow the extraction of cross sections.

The Maxwell-Boltzman distribution in the moving frame can be written as

$$\frac{d^2\sigma}{dE^*\Omega^*} = \frac{\sigma_i}{2(\pi\tau_i)^{3/2}} \sqrt{E^*}\, e^{-E^*/\tau_i} \tag{4}$$

where E* is the kinetic energy available in the two-body break up, σ_i is the cross section, and τ_i is the temperature. The correction for the recoil of the residual nucleus is made by multiplying the energy by

$$\nu = A_T/(A_T-A) \tag{5}$$

where A and A_T are the mass numbers of the fragment and the nucleus which is assumed to break up, respectively. The Coulomb barrier penetration factor, $1 - kB/(\nu E)$, should multiply $\sqrt{E^*}$ in equation 4. However, this makes the normalization very cumbersome. As will be shown below it makes very little difference and is easier to simply shift the energy by kB as

$$E^* = \nu E' - \langle k \rangle_i B \tag{6}$$

$$B = \frac{Z(Z_T-Z)e^2}{1.44\ [A^{1/3} + (A_T-A)^{1/3}]}$$

where E' is the kinetic energy in the frame which will be assumed to be moving with velocity β_i with respect to the lab, Z and Z_T are the atomic numbers of the fragment and of the nucleus assumed to break up, respectively,

and $\langle k \rangle_i$ is the nominal barrier fraction. The energy distribution in the moving frame becomes

$$\frac{d^2\sigma}{dE'd\Omega'} = \frac{1}{2\Delta} \int_{k=\langle k \rangle_i - \Delta}^{k=\langle k \rangle_i + \Delta} \frac{\nu\sigma_i}{2(\pi\tau_i)^{3/2}} (\nu E' - kB)^{1/2} e^{-(\nu E' - kB)/\tau_i} dk \qquad (E' > kB/\nu) \qquad (\Delta \leq \langle k \rangle_i) \qquad (7)$$

where Δ is the smearing parameter. If smearing is not used, the integration over k should be ignored, and the expression evaluated at $k = \langle k \rangle_i$. The mean of this expression is $(3\tau/2 + kB)/\nu$ and the maximum occurs at $(\tau/2 + kB)/\nu$. The laboratory distributions are found by transforming from the moving frame and summing the two components,

$$\frac{d^2\sigma}{dEd\Omega} = \sum_{i=1,2} (E/E')^{1/2} \frac{d^2\sigma}{dE'\Omega'} \qquad (8)$$

$$E' = E + \frac{1}{2}m\beta_i^2 - \beta_i(2mE)^{1/2} \cos\theta_{lab}$$

where E is the laboratory fragment kinetic energy and m is the fragment mass.

Thus, the parameters to be determined are β_1, β_2, τ_1, τ_2, $\langle k \rangle_1$, $\langle k \rangle_2$, σ_1, σ_2, and Δ. The parameters σ_1 and σ_2 are more easily discussed in terms of the overall normalization, A, and the ratio between the two cross sections, R,

$$A = \sigma_1 + \sigma_2$$
$$R = \sigma_2/\sigma_1 \quad . \tag{9}$$

The index 1 is identified with the low energy, low β, low τ part of the spectra, while index 2 refers to the high energy, high β, high τ part of the spectra. The general method of adjusting parameters is as follows. The emitting nucleus is known, fixing Z_T and A_T. For the Ag and U targets, the emitting nucleus was selected in accordance with Refs. 1 and 3, where the breakup was taken to occur after a fast cascade stage which ejected several nucleons, leaving an excited residual nucleus. The residual nuclei were taken to be ^{96}Tc and ^{220}Rn for Ag and U respectively. The target was taken as the emitting nucleus in the case of C and Al. The two temperatures, t, and barrier fractions, $\langle k \rangle$, are adjusted at 90° with the two velocities, β, then being adjusted to reproduce the spread between the 20° and 160° spectra. The ratio of high energy to low energy cross reactions, R, is then adjusted so that the sum of the two different distributions add up to give the correct shape of the spectra. Smearing, Δ, is introduced if necessary. Some iteration is necessary to achieve good visual fits to the data.

The fitted parameters for the measured fragments from C, Al, Ag and U targets are given in Table III and Table IV. Since no isotopic resolution was obtained, the mass of the fragment was assumed to be that of the most stable isotope. However, in the case of the heavier fragments from C, there was a very strong dependence of the functional form on the fragment mass and thus the calculations were summed over the isotopes in this case only.[41]

V. PARAMETER FITS TO THE DATA

The solid lines in Figs. 2, 3, 5, 8, 9, 10 represent the calculations done with the parameters as given in Tables III and IV. For the most part the fits are quite reasonable. For the Al target in Fig. 5 the increasing steepness of the curves with increasing Z is explained with a constant temperature (see Table III) by the two body kinematics. For the Ag target in Fig. 8 the surprising shift of the peak energy is also explained by the two body kinematics.

However, in Fig. 9 the curves have a hump on the high side of the peak which is not in the data. This is because of the rectangular smearing function with width 2Δ which was used. Probably a better procedure would have been to accomplish the smearing by performing a convolution with a Gaussian whose FWHM was 0.68 times 2Δ. Although the low-temperature barrier fraction, $\langle k \rangle_1$, is determined to be zero for carbon by the data of Greiner et al[5], the turnover of the lowest energy points in Fig. 5 for He and Li fragments indicates a non zero value of $\langle k \rangle_1$ for aluminum as shown in Table III. Figure 10 shows that the fragments from the heavy targets have a more forward peaked angular distribution than the model allows, as has been pointed out previously.[3]

In Fig. 11, the fit to the ^{7}Be energy spectra given in Fig. 3 is transformed to $p_{\parallel}$ using the equation

$$\frac{d^3\sigma}{dp_\perp\, dp_\parallel\, d\phi} = \frac{\sin\theta}{m}\,\frac{d^2\sigma}{dE d\Omega} \tag{10}$$

and integrating over $p_\perp$ and ϕ. Note that this fit to the entire energy spectrum, when displayed vs $p_\parallel$, deviates somewhat from the Gaussian fit at high $|p_\parallel|$ where the high energy tail contributes to the energy spectra. This discrepancy is also evident in Fig. 2 where it can be seen that our data lie above the dashed lines which represent the data of Greiner et al.[5] This may be because the small angular acceptance of their spectrometer somewhat reduced the efficiency for the larger transverse momentum fragments.

By comparing equations (3) and (7)-(8) one can see that

$$\tau = \nu \, \sigma^2_{p_\parallel} / m \tag{11}$$

$$\beta = \langle p_\parallel \rangle / m \quad . \tag{12}$$

Therefore the dependence of the widths, $\sigma_{p_\parallel}$, of these momentum distributions can be obtained from eq. (5) and (11) as

$$\sigma_{p_\parallel} = \sqrt{m_o} \, [A(A_T - A)\tau/A_T]^{1/2} \quad , \tag{13}$$

where m_o is the nucleon mass. This equation has been derived by Goldharber.[42] When compared to the dependence first reported by Greiner et al,[5]

$$\sigma_{p_\parallel} = \sigma_o [4A(A_T - A)/A_T^2]^{1/2} \tag{14}$$

it can be seen that the fragment mass dependence is the same, but that the target (or projectile) mass dependence is somewhat different. In fact, in comparing the fragmentation of carbon and oxygen Greiner et al[5]

found that σ_o of eq. (14) was not constant but that τ of eq. (13) was constant, as is also found to be approximately true when comparing the carbon and aluminum parameters in Table III.

The interpretation of the low temperature component may be that it results from the Fermi momentum in the nucleus which is breaking up. This has been pointed out by Goldhaber[42] and again recently by Gelbke et al.[43] They show that the temperature is then related to the Fermi momentum, p_F, by

$$\tau = p_F^2/(5\ m_o) \quad . \tag{15}$$

A Fermi momentum of 200 MeV/c would correspond to a temperature of 8.6 MeV, which is of the order of the observed low temperature components. Such an explanation is then also consistent with the limiting fragmentation and factorization concepts observed in projectile fragmentation. For the high temperature component which dominates for heavy targets the concept of factorization is clearly not applicable.[38]

The U data in Fig. 9 were also fit with the old functional form[3] which has a preexponential term of E instead of $\sqrt{E}$. The fitted temperatures were the same because they are insensitive to the preexponential term. However with the present functional form the <k> and Δ values are about 15% larger. Comparing with the proper barrier penetration factor, 1-kB/(νE), with the $\sqrt{E}$ preexponential, the differences would be in the same direction but even smaller. Thus the value of 0.3 for the barrier fraction given for the silver data in Table IV is surprisingly low, independent of functional form.

In order to test the range of validity of the new functional form a few other examples of data from the literature have been fit with it. The counter telescope measurements[22] of Li from Ni at 60° were nicely fit with only the high temperature component. The emitting nucleus was chosen as ^{54}Fe and β_2 as 0.008. The parameters fit were τ_2 = 14 MeV, $\langle k \rangle_2$ = 0.35, and Δ = 0.2, as one would interpolate from Tables III and IV. The ^{24}Na from Bi radiochemical measurements[27] at 90° were perfectly fit with τ_2 = 14.5 MeV, $\langle k \rangle_2$ = 0.4 and Δ = 0.28 as one would expect from Table IV. (The emitting nucleus was taken to be ^{195}Pt as in the original work.[27]) From the forward and backward angle shift of the energy spectra a value of $\beta = 0.0066 \pm 0.0009$ had been deduced[27] which also agrees nicely with Table IV. The momentum spectra of high energy fission fragments[44] are nearly Gaussian and therefore might also be fit with the present functional form.

The cases we have considered so far are either the breakup of a light system or fragment production from a heavy target. In both instances the approximation of two body kinematics which we use seems reasonable. Let us now consider some cases where this is obviously not reasonable: spallation residues formed from multiparticle emission. In the differential range measurements[17] of ^{24}Na from Al the peak position is surprisingly fit by a $\langle k \rangle$ of 0.45 as in Table III, although this reaction is clearly not a two body breakup. However, the ^{24}Na recoil energy has long been thought to be anomalously large[17,20] and is still not understood. For this reaction, the β values deduced[17,20] are about 0.003, considerably smaller than those in Table III. Lastly,

let us consider a deep spallation reaction: ^{149}Tb from Au. The average recoil energy[45] is about half what is calculated by the present formalism showing the limitation of the method.

It has long been known[3] that the energy spectra of the lightest fragments from heavy targets exhibit a break at high kinetic energy, with the flattening of the spectra indicating still higher apparent temperatures of about 20 MeV. This was particularly evident for the neutron deficient isotopes which are the lightest isotopes of each element. This effect is several orders of magnitude more prominent in irradiations with relativistic heavy ions,[38] and has recently been satisfactorily described by the coalescence of cascade nucleons[46] or by nucleosynthesis in the fireball.[47] Even near the evaporation peak for light fragments from a uranium target the apparent temperatures are considerably higher when the reaction is induced by relativistic heavy ions.[38]

VI. CROSS SECTIONS

The integrated cross sections are of considerable interest. For the uranium target the energy spectra were sufficiently complete that, with small extrapolations, they could be integrated, and the resulting angular distributions integrated. The cross sections obtained from uranium are shown in Table V together with those previously obtained[3] for the lighter fragments. For the silver data it was necessary to extrapolate to lower energies using the functional form described in the previous section and, because measurements were only made at 90°, it was necessary to assume that the cross section was 4π times the 90° value. This is a valid assumption as long as the angular distribution is symmetric about 90° in the laboratory, which is generally the case. These cross sections together with some from our previous work,[1] and some fits to our previous data,[1] are given in Table V. Also indicated is the fraction of the cross section which was experimentally measured. The same fitted cross sections and fraction measured are given for the aluminum target. This represents almost the entire charge yield curve for the spallation of aluminum. However, from the known activation data on the production of ^{22}Na and ^{24}Na the cross sections must increase at higher Z. In fact the O to Ne cross sections are probably low because of the inability to fit the low temperature component. Indeed, the sum of the cross sections from Li through Ne is only 177 mb, which is less than half of the total reaction cross section of 400 mb.[48] For the carbon target the integrated cross sections reflect mainly the data of Greiner et al,[5] but include the contribution of the high energy tails measured in this work. Also the data have been

renormalized to agree with the ^{7}Be activation measurement[34,35] and therefore differ slightly from Lindstrom et al.[39]

All four charge yield curves are shown in Fig. 12. There appears to be an odd-even effect in Z, especially for the Al target. Also the yield of beryllium is low because of the particle instability of ^{8}Be as noted previously.[3]

VII. CONCLUSIONS

A uniform treatment of the energy spectra of nuclear fragments from both light and heavy targets, as well as from projectile fragmentation, has been attempted here. The data are consistently described as the sum of two Maxwellian distributions. These distributions are shifted along the beam direction by velocities, β, of 0.002 to 0.013 in units of c. The nominal Coulomb barrier fractions, $\langle k \rangle$, when compared to tangent spheres with a radius parameter of 1.44 fm, are 0.3 to 0.55. The low temperature Maxwellian has a temperature of 4.5 to 7.5 MeV, but is suppressed by the Coulomb barrier for the heavy targets. For all the targets there is a high temperature component with temperature of 12 to 16 MeV. The average parameters for each target are given in Table VI.

Two body kinematics was incorporated into the functional form of the fitting procedure. This does not imply that there are only two products in every final state. For the heavy fragments from heavy targets, several nucleons accompanying the fragment would not affect the essentially two body character of the break up, especially if the nucleons are emitted from the other body. For the light targets it is clear the highest energy fragments must come from two body break ups. Although these may represent a small fraction of the total cross section, they will dominate the high energy parts of the energy spectra, where the two body assumption is most necessary.

In order to obtain a consistent treatment it was necessary to use a Maxwellian distribution function with a pre-exponential factor of $\sqrt{E}$, in contrast to the pre-exponential factor of E derived by Weisskopf[50]

forty years ago. The pre-exponential factor has been clearly determined by the data of Greiner et al.[5] for light systems as $\sqrt{E}$. For the heavy systems the strong effect of the Coulomb barrier makes it difficult to distinguish between these two forms, thus allowing $\sqrt{E}$ to be an adequate description for all systems. Goldhaber[51] points out that the $\sqrt{E}$ function is a Maxwellian distribution inside a volume, and the E function of Weisskopf contains an extra velocity factor for the emission from a surface. Thus the $\sqrt{E}$ function is reasonable for the breakup of a light system[5] and for the nuclear fireball.[38] The E function is more reasonable for the evaporation from the surface of a heavy system, but in practice is not significantly different because of the effect of the Coulomb barrier.

Because the targets used in this study span the range from light to heavy nuclei the results may be used to unify the pictures of target and projectile fragmentation, which have previously appeared to be two quite distinct processes. The differences arise because the low temperature component is dominant in the spallation of light targets and the projectile fragmentation studies which have been done so far. The high temperature component is dominant in the fragmentation of heavy targets. However, both components are evident in the data from the aluminum target, and even for the carbon target, there is a small amount of the high temperature component which was missed in the measurements of Greiner et al.[5] The low temperature component may be interpreted as the Fermi momentum due to a sudden break up process, while the high temperature component is surely the result of high deposition energies in the emitting nucleus. The low temperature

component may also be thought of as resulting from peripheral collisions which dominate for light nuclei, and the high temperature component as resulting from central collisions. For heavy nuclei peripheral collisions do not give rise to the fragments studied here, but probably emit only a few nucleons, or fission in the case of uranium. The apparent limiting temperature of about 8 MeV observed in projectile fragmentation studies,[49] is because the projectiles have not yet been heavy enough to observe the high temperature component.

ACKNOWLEDGMENTS

This research was supported by the U.S. Department of Energy. We are grateful for help from D. A. Landis, M. M. Fowler, R. C. Jared, L. F. Archambault, R. D. Giauque, and the Bevatron staff. Helpful discussions with H. Crawford, J. B. Cumming, A. S. Goldhaber, J. Gosset, P. J. Lindstrom, W. G. Meyer, S. A. Nissen-Meyer, and L. P. Remsberg are also appreciated.

*Present address: Department of Laboratory Services, Veterans Administration Hospital, Martinez, CA 94553.

‡Present address: Los Alamos Scientific Laboratory, Los Alamos, NM 87545.

REFERENCES

1. E. K. Hyde, G. W. Butler, and A. M. Poskanzer, Phys. Rev. C4, 1759 (1971).

2. R. G. Korteling, C. R. Toren, and E. K. Hyde, Phys. Rev. C7, 1611 (1973).

3. A. M. Poskanzer, G. W. Butler, and E. K. Hyde, Phys. Rev. C3, 882 (1971).

4. A. M. Zebelman, W. G. Meyer, K. Halbach, A. M. Poskanzer, R. G. Sextro, G. Gabor, and D. A. Landis, Nuc. Instrum. Methods 141, 439 (1977).

5. D. E. Greiner, P. J. Lindstrom, H. H. Heckman, B. Cork, and F. S. Bieser, Phys. Rev. Lett. 35, 152 (1975).

6. S. Katcoff, Phys. Rev. 114, 905 (1959).

7. S. A. Azimov, R. Aripov, E. V. Beter, U. G. Gulyamov, K. Igamberdiev, and O. V. Lozhkin, Sov. J. Nuc. Phys. 10, 652 (1970).

8. J. A. Panontin, L. L. Schwartz, A. F. Stehney, E. P. Steinberg, and L. Winsberg, Phys. Rev. 169, 851 (1963).

9. N. M. Hintz, Phys. Rev. 86, 1042 (1952).

10. S. Singh and J. M. Alexander, Phys. Rev. 128, 711 (1962).

11. J. P. Alard, A. Baldit, R. Brun, J. P. Costilhes, J. Dhermain, J. Fargeix, L. Fraysse, J. Pellet, G. Roche, J. C. Tamain, Nuovo Cimento 30A, 320 (1975).

12. R. D. Edge, Bull. Am. Phys. Soc. 21, 29 (1976).

13. C. N. Davids, H. Laumer, and S. M. Austin, Phys. Rev. Lett. 22, 1388 (1969).

14. C. T. Roche, R. G. Clark, G. J. Mathews, and V. E. Viola, Jr., Phys. Rev. C14, 410 (1976).

15. V. I. Bogatin, V. F. Litvin, O. V. Lozhkin, N. A. Perfilov, and Yu P. Yakovlev, Nucl. Phys. A260, 446 (1976).

16. V. E. Dudkin, V. N. Kuz'min, L. N. Smirennyi, N. S. Shimanskaya, and R. M. Yakovlev, Sov. J. Nucl. Phys. 9, 541 (1969).

17. A. M. Poskanzer, J. B. Cumming, and R. Wolfgang, Phys. Rev. 129, 374 (1963).

18. F. P. Denisov, V. P. Milovanov, V. N. Pokrovskii, P. A. Cerenkov, and I. A. Yutlandov, Sov. J. Nucl. Phys. 9, 544 (1969).

19. E. P. Steinberg, and L. Winsberg, Phys. Rev. C10, 1925 (1974).

20. S. K. Chang and N. Sugarman, Phys. Rev. C, to be published (1977).

21. G. A. Fedosleev, L. P. Moskaleva, and B. Ya. Shcherbovskii, Sov. J. Nucl. Phys. 9, 675 (1969); L. P. Moskaleva, G. A. Fedoseev, and B. Ya. Shcherbovskii, Bull. Acad. Sci. USSR, Phys. Ser., 32 648 (1968); L. P. Moskaleva and A. K. Lavrukhina, Bull. Acad. Sci. USSR, Phys. Ser., 27, 1248 (1963).

22. G. M. Raisbeck, P. Boerstling, R. Klapisch, and T. D. Thomas, Phys. Rev. C12, 527 (1975).

23. E.N. Volnin, G. M. Amalsky, D. M. Seleverstov, N. N. Smirnov, A. A. Vorobyov, and Yu. P. Yakovlev, Phys. Lett. 55B, 409 (1975).

24. E. N. Vol'nin, A. A. Vorob'ev, and D. M. Seliverstov, JETP Lett., 19, 357 (1974); E. N. Vol'nin, A. A. Vorobyov, V. T. Grachov, D. M. Seleverstov, and E. M. Spiridenkov, Leningrad Institute of Nuclear Physics Report #101, (unpublished) 1974.

25. L. P. Remsberg and D. G. Perry, Phys. Rev. Lett. 35, 361 (1975).

26. G. W. Butler, D. G. Perry, A. M. Poskanzer, J. B. Natowitz, F. Plasil, and L. P. Remsberg, VI International Conference on High Energy Physics and Nuclear Structure, Santa Fe (1975); and unpublished.

27. J. B. Cumming, R. J. Cross Jr., J. Hudis, and A. M. Poskanzer, Phys. Rev. 134, B167 (1964).

28. J. B. Cumming, S. Katcoff, N. T. Porile, S. Tanaka, and A. Wyttenbach, Phys. Rev. 134, B1262 (1964).

29. N. T. Porile and S. Tanaka, Phys. Rev. 137, B58 (1965).

30. S. B. Kaufman and M. W. Weisfield, Phys. Rev. C11, 1258 (1975).

31. M. M. Fowler and R. C. Jared, Nucl. Instrum. Methods 124, 341 (1975).

32. W. P. Jesse, Phys. Rev. 174, 173 (1968).

33. G. W. Butler, A. M. Poskanzer and D. A. Landis, Nucl. Instrum. Methods 89, 189 (1970).

34. J. B. Cumming, J. Hudis, A. M. Poskanzer, and S. Kaufman, Phys. Rev. 128, 2392 (1962).

35. A. F. Stehney and E. P. Steinberg, Nucl. Phys. B5, 188 (1968).

36. J. B. Cumming, Ann. Rev. Nucl. Sci. 13, 261 (1963).

37. The technique of studying proton-nucleus elastic scattering by recoil detection has been successfully tested for the case of a ^{7}Li target. A. M. Poskanzer, A. M. Zebelman, and V. Viola, LBL Report No. LBL-2366, p. 127, 1974 (unpublished).

38. J. Gosset, H. H. Gutbrod, W. G. Meyer, A. M. Poskanzer, A. Sandoval, R. Stock, and G. D. Westfall, Phys. Rev. C. 16, 629 (1977).

39. P. J. Lindstrom, D. E. Greiner, H. H. Heckman, B. Cork, and F. S. Bieser, Lawrence Berkeley Lab Report No. LBL 3650, (unpublished) (1975).

40. B. Jakobsson, R. Kullberg and I. Otterlund, Lettere al Nuovo Cimento 15, 444 (1976).

41. For ^{9,10}Be from C, 63% was taken to be ^{9}Be and 37% was taken to be ^{10}Be, in accordance with the projectile fragmentation data.[39] For B, the fractions were 17% ^{8}B, 29% ^{10}B, and 54% ^{11}B. For C, the percentages were 29% ^{9}C, 6% ^{10}C, and 65% ^{11}C.

42. A. S. Goldhaber, Phys. Lett. 53B, 306 (1974).

43. C. K. Gelbke, D. K. Scott, M. Bini, D. L. Hendrie, J. L. Laville, J. Mahoney, M. C. Mermaz, and C. Olmer, Phys. Letters , (1977).

44. V. P. Crespo, J. B. Cumming, and A. M. Poskanzer, Phys. Rev. 174, 1455 (1968).

45. V. P. Crespo, J. B. Cumming, and J. M. Alexander, Phys. Rev. C2, 1777 (1970).

46. H. H. Gutbrod, A. Sandoval, P. J. Johansen, A. M. Poskanzer, J. Gosset, W. G. Meyer, G. D. Westfall, and R. Stock, Phys. Rev. Lett. 37, 667 (1976).

47. A. Mekjian, Phys. Rev. C, to be published (1977).

48. R. W. Williams, Rev. Mod. Phys. 36, 815 (1964).

49. D. K. Scott, private communication (1977).

50. V. Weisskopf, Phys. Rev. 52, 295 (1937).

51. A. S. Goldhaber, Phys. Rev. C , (1977). LBL-7146

TABLE I. Recent counter telescope studies of nuclear fragments produced by high energy protons.

Targets	Proton Energy (GeV)	Fragments	Ref.
C,Al,Au	0.6	H,He	11
B,Ni,Sn,Sm	0.66	H-Be	15
Ni	3.0	Li-B	22
Ti,Ni,Sn	1.0	He-C	23
Ag,Au,U	1.0	He-B	24
Au,U	28	C-Mg	25
U	0.8	He-B	26

TABLE II. Silicon counter telescopes. The numbers given are the thicknesses in μm of the ΔE and E detectors, followed in parenthesis by the lower discriminator setting in MeV of the E counter.

Isotope \ Target	CH $0.41\ mg/cm^2$	Al $1.1\ mg/cm^2$	Al $3.3\ mg/cm^2$
$1\text{-}3_H$			61-250(2.2),100-1500(2),250-5000(5)
^3He, ^4He	22-410(0.8)	20-168(3)	61-250(2.2),100-1500(2),250-5000(5)
^6He, $6\text{-}9_{Li}$		20-168(3)	61-250(2.2)
$7,9,10_{Be},8,10\text{-}12_{B,C}$		20-168(7)	61-250(5)

TABLE III. Fitted parameters of functional form (see text) for energy spectra of fragments from C and Al targets.

Target	Product	β_1	τ_1	$\langle k \rangle_1$	β_2	τ_2	$\langle k \rangle_2$	R
C	^{4}He	0.0067[a]	4.5	0.0	0.013	13	0.45	0.8
	Li	0.006[a]	5.5	0.0	0.013	14	0.45	1.5
	^{7}Be	0.0075[a]	5.5	0.0	0.013	14	0.45	1.0
	^{9}Be	0.0045[a]	6.0	0.0	0.013	14	0.45	2.0
	^{10}Be	0.0032[a]	6.0	0.0	0.013	14	0.45	2.0
	^{8}B	0.0052[a]	6.5	0.0	0.013	14	0.45	2.0
	^{10}B	0.0038[a]	6.5	0.0	0.013	14	0.45	2.0
	^{11}B	0.0022[a]	6.5	0.0	0.013	14	0.45	2.0
	^{9}C	0.0051[a]	7.0	0.0	0.013	14	0.45	2.0
	^{10}C	0.0045[a]	7.0	0.0	0.013	14	0.45	2.0
	^{11}C	0.0039[a]	7.0	0.0	0.013	14	0.45	2.0
Al	^{4}He	0.005	4	0.45	0.008	12	0.45	0.7
	Li	0.005	7.5	0.45	0.008	12	0.45	2.0
	^{7}Be	0.005	7.5	0.45	0.008	12	0.45	2.0
	^{9,10}Be	0.005	7.5	0.45	0.008	12	0.45	0.5
	B	0.005	7.5	0.45	0.008	12	0.45	1.3
	C	0.005	7.5	0.45	0.008	12	0.45	0.7
	N	0.005	7.5	0.45	0.008	12	0.45	0.7
	O	-	-	-	0.008	12	0.45	-
	F	-	-	-	0.008	12	0.45	-
	Ne	-	-	-	0.008	12	0.45	-

[a]From Ref. 5.

TABLE IV. Fitted parameters of functional form (see text) for energy spectra of fragments from Ag and U targets.

Target	Product	β_2	τ_2	$\langle k \rangle_2$	Δ
Ag	B[a]	-	15	0.3	0.3
	C[a]	-	15	0.3	0.3
	N[a]	-	15	0.3	0.3
	O	-	15	0.3	0.3
	F	-	15	0.3	0.3
	Ne	-	15	0.3	0.3
	Na	-	16	0.3	0.28
	Mg	-	16	0.3	0.28
	Al	-	16	0.3	0.28
	Si	-	16	0.3	0.28
	P	-	16	0.3	0.28
	S	-	16	0.3	0.28
	Cl	-	16	0.3	0.28
	Ar	-	16	0.3	0.28
U	F	0.006	14	0.55	0.28
	Ne	0.006	14	0.55	0.30
	Na	0.006	14	0.54	0.28
	Mg	0.006	14	0.54	0.30
	Al	0.006	14	0.53	0.28
	Si	0.006	14	0.48	0.30
	P	0.006	14	0.49	0.28
	S	0.006	14	0.49	0.30
	Cl	0.006	14	0.50	0.28
	Ar	0.006	14	0.51	0.30

[a]Fit to data from Ref. 1.

TABLE V. Cross-sections in mb for fragments produced by irradiation with 4.9 GeV protons. The percent of the total cross section which was measured is given in parentheses. At 2.1 GeV the Al cross sections are the same but the carbon cross sections should be raised by the factor 10/9.4.

Product \ Target	C	Al	Ag	U
He	167.[d]	414.[d] (95)	2390.[a]	4400.[c]
Li	24.	31. (95)	139.[a]	301.[c]
^{7}Be[e]	[9.4]	[8.4] (90)	[17.4[a]]	[17.6[c]]
^{9,10}Be	8.6	6.9 (80)	25.5[a]	110.[c]
B	43.	20. (80)	62.[b] (40)	117.[c]
C	27.	31. (65)	74.[b] (40)	96.[c]
N		22. (50)	46.[b] (60)	64.[c]
O		28. (25)	35.[f] (85)	47.[c]
F		14. (15)	31.[f] (85)	28.
Ne		16. (10)	31.[f] (80)	25.
Na			14.[f] (80)	22.
Mg			8.3[f] (80)	27.
Al			10.1[f] (65)	22.
Si			8.5[f] (65)	24.
P			6.2[f] (60)	22.
S			6.3[f] (60)	23.
Cl			5.8[f] (40)	20.
Ar			5.4[f] (40)	21.

[a] From Ref. 1.

[b] From fit to data from Ref. 1.

[c] From Ref. 3.

[d] ^{4}He only.

[e] Radiochemical measurements used for normalization.

[f] Obtained from the 90° differential cross section by multiplying by 4π.

TABLE VI. Average values of the parameters β, the velocity of the emitting system, τ, the temperature, and $\langle k \rangle$, the nominal barrier fraction, for the low (1) and high (2) temperature components.

Target	β_1	τ_1(MeV)	β_2	τ_2(MeV)	$\langle k \rangle_2$
C	0.005	6.5	0.013	14	0.45
Al	0.005	7.5	0.008	12	0.45
Ag	-		0.006[a]	$15\frac{1}{2}$	0.3
U	-		0.006	14	0.5

[a]From Ref. 1.

FIGURE CAPTIONS

Fig. 1 Data obtained from an Al target with the telescope utilizing gas ΔE and silicon E counters. a. Two-dimensional plot of ΔE vs E showing distinct ridges for the different elements. The valleys between elements have been adjusted to zero in order to make the ridge lines clear. b. Analogue particle identifier spectrum for fragments with energies between 5 and 10 MeV.

Fig. 2 Measured energy spectra at 90° in the laboratory for fragments from a C target irradiated by 2.1 GeV protons using the gas telescope. The ^{4}He spectrum above 6 MeV was measured with a silicon telescope. The dashed lines represent the 2.1 GeV/nucleon C on hydrogen fragmentation data of Ref. 5. The solid lines are fits to the spectra using the functional form described in the text with the parameters given in Table III.

Fig. 3 Energy spectra of ^{7}Be fragments from a C target bombarded with 2.1 GeV protons measured at 20, 90, and 160° in the laboratory. The dashed and solid lines have the same meaning as those in Fig. 2 . The solid lines are normalized at 90° only.

Fig. 4 Measured energy spectra of individual isotopes at 90° in the laboratory from an Al target irradiated by 4.9 GeV protons using a silicon telescope to obtain isotope resolution. The ^{4}He and ^{7}Be spectra have been extended down to lower energies using the gas telescope data.

Fig. 5 Measured energy spectra of the different elements and ^{4}He and ^{7}Be at 90° in the laboratory from an Al target irradiated by 4.9 GeV protons using the gas telescope to measure the low energy part of the spectra and a silicon telescope to measure the higher energy part of the spectra for elements up to carbon. The solid lines correspond to fits to the spectra using the functional form described in the text with the parameters given in Table III. The dashed line for Na is to guide the eye.

Fig. 6 Energy spectra in the laboratory of protons and ^{4}He fragments from an Al target irradiated by 4.9 GeV protons.

Fig. 7 Energy spectra in the laboratory of Li and Na fragments from an Al target irradiated by 4.9 GeV protons. The back angle data for Na were not statistically significant enough to plot.

Fig. 8 Measured energy spectra at 90° in the laboratory for fragments from an Ag target irradiated by 4.9 GeV protons. Each successive element is suppressed by a factor of 2. The dashed line corresponds to data from Ref. 1. The solid lines are fits to spectra using the functional form described in the text using parameters from Table IV.

Fig. 9 Measured energy spectra at 90° in the laboratory for fragments from a U target irradiated by 4.9 GeV protons. Each successive element is suppressed by a factor of 2. The solid lines are fits to the spectra using the functional form described in the text with parameters from Table IV. At low energies, where this functional form is not applicable, the dashed lines are to guide the eye through the data.

Fig. 10 Energy spectra of Na fragments from a U target bombarded with 4.9 GeV protons measured at 20, 90, and 160° in the laboratory. The solid lines are fits to the spectra, normalized at 90° only, using the functional form described in the text with parameters from Table IV.

Fig. 11 Measured momentum distribution of ^{7}Be fragments from the fragmentation of 2.1 GeV/nucleon ^{12}C on a hydrogen target from Ref. 5. The dashed line represents their Gaussian fit to the data with σ_o = 8.8 mb, $\sigma_{p_{||}}$ = 145 MeV/c and $\langle p_{||} \rangle$ = -49 MeV/c. The solid line stands for the transformation to momentum space of the functional form described in the text which fit the measured energy spectra of ^{7}Be fragments from a C target irradiated by 2.1 GeV protons.

Fig. 12 Cross sections as a function of Z for the four targets studied. More information is given in Table V.

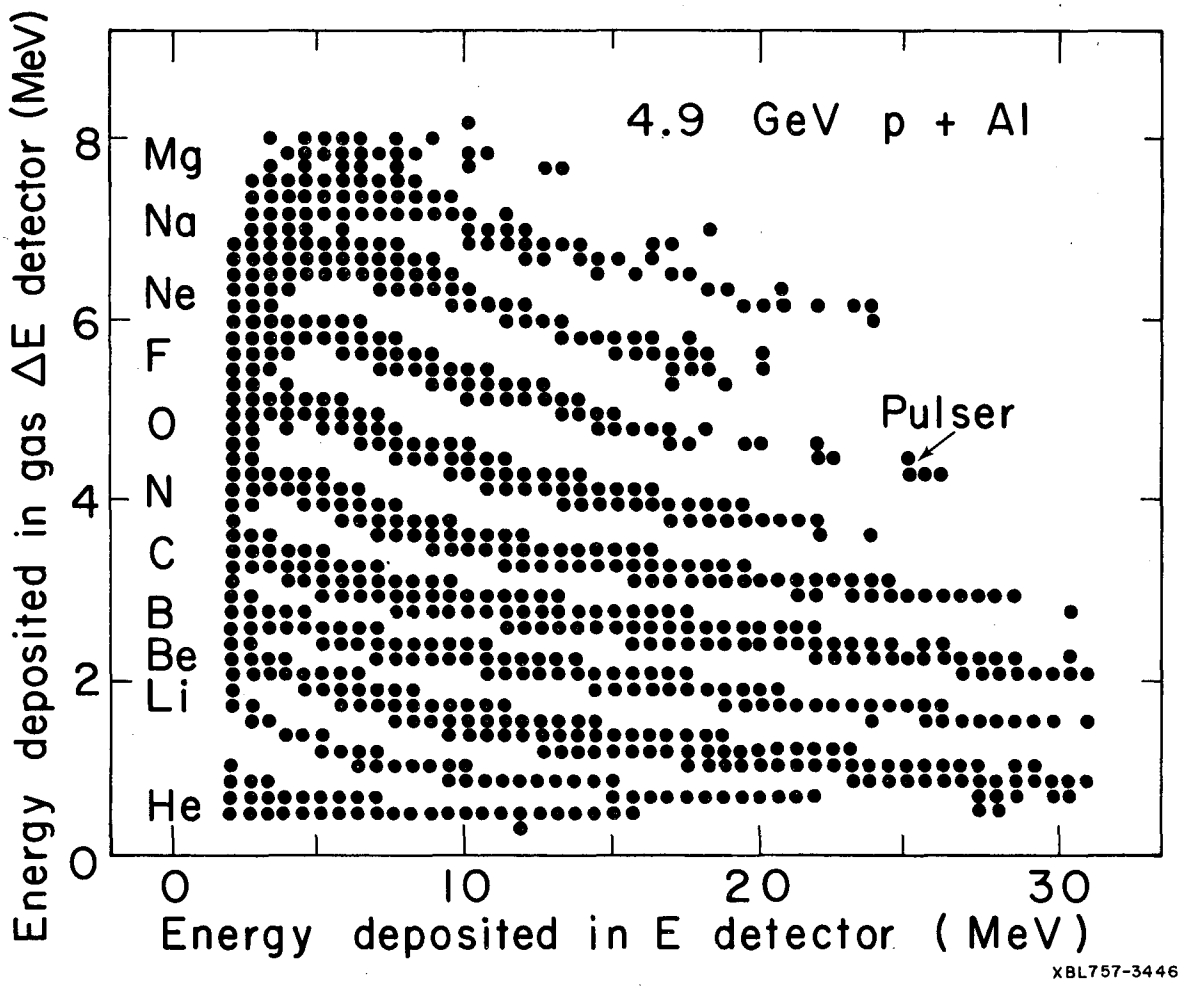

Fig. 1a

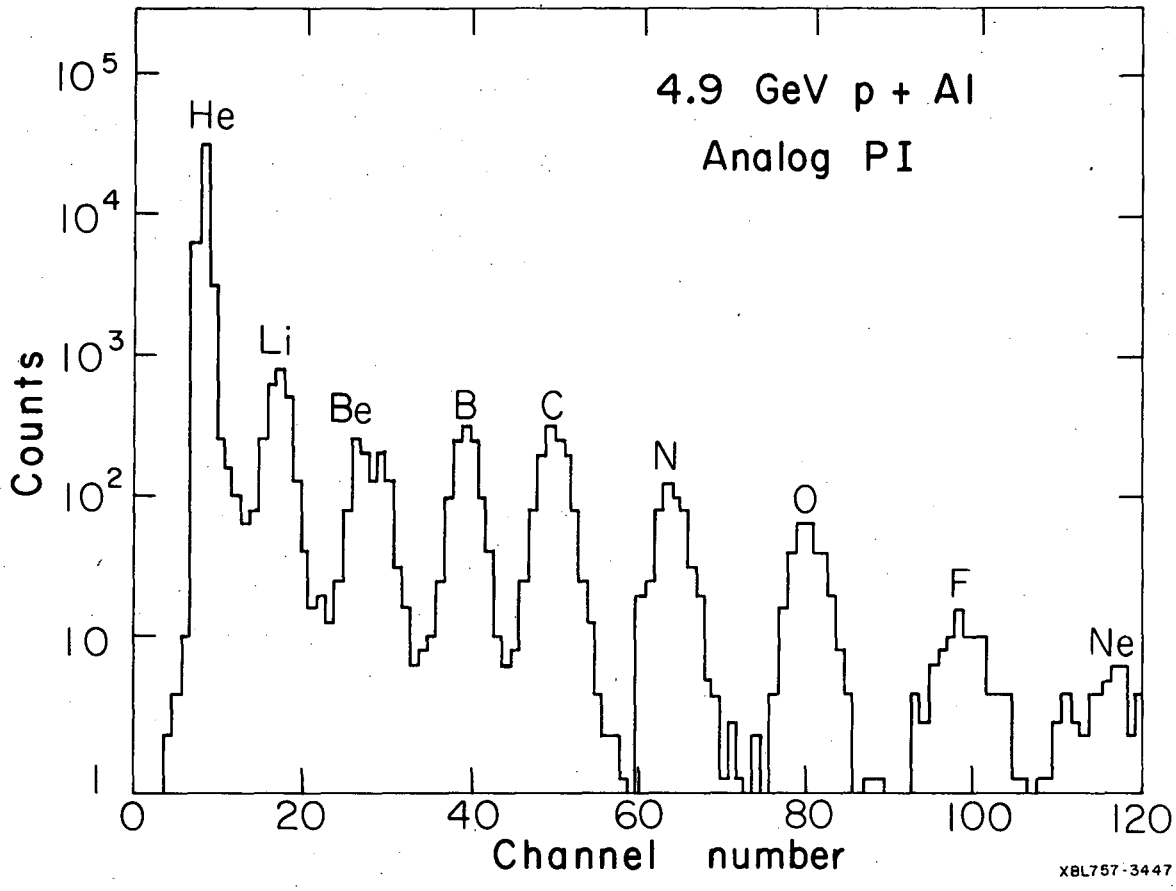
4.9 GeV p + Al
Analog PI
Counts
Channel number
He
Li
Be
B
C
N
O
F
Ne
10^5
10^4
10^3
10^2
10
1
0
20
40
60
80
100
120
XBL757-3447

Fig. 1b

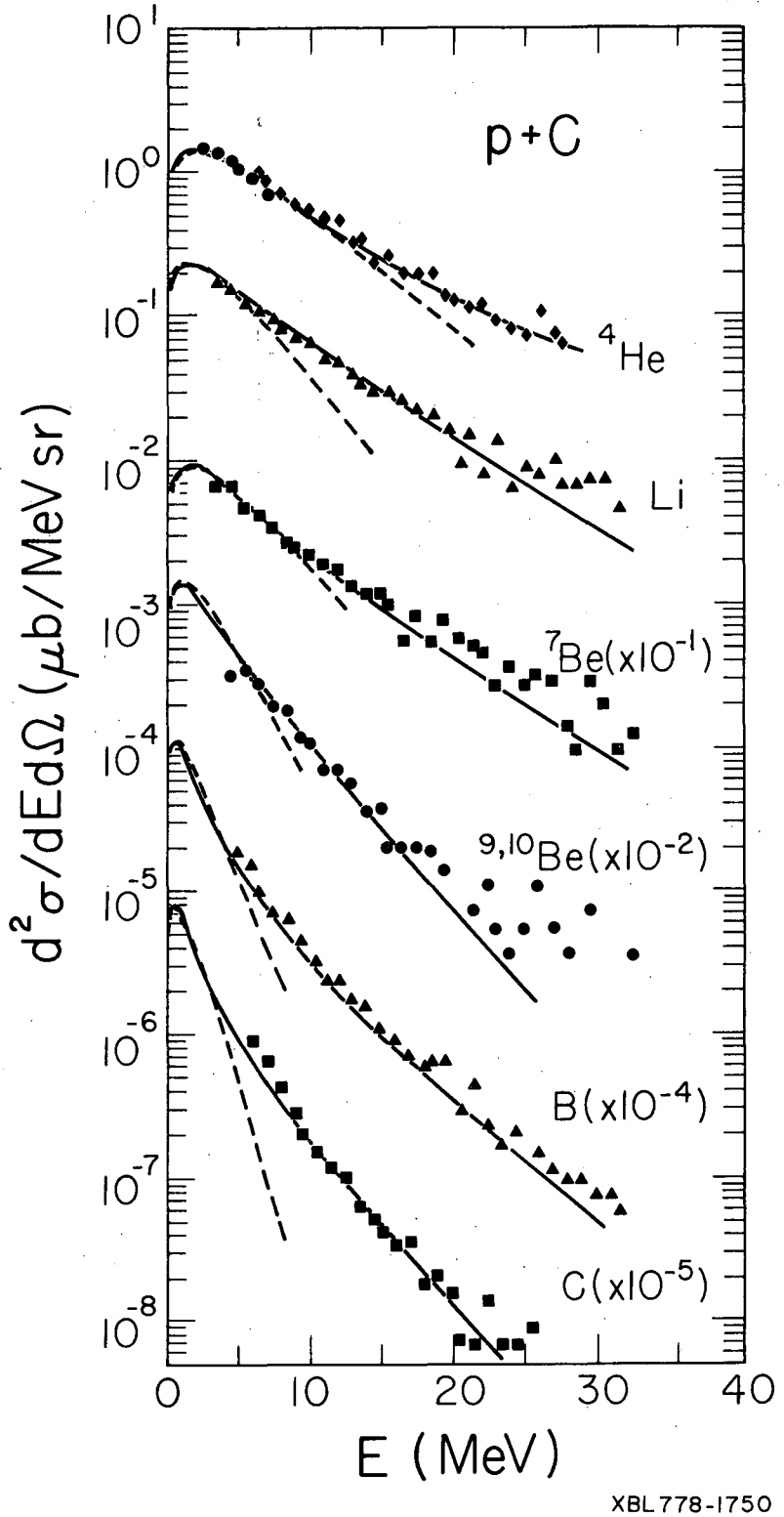

Fig. 2

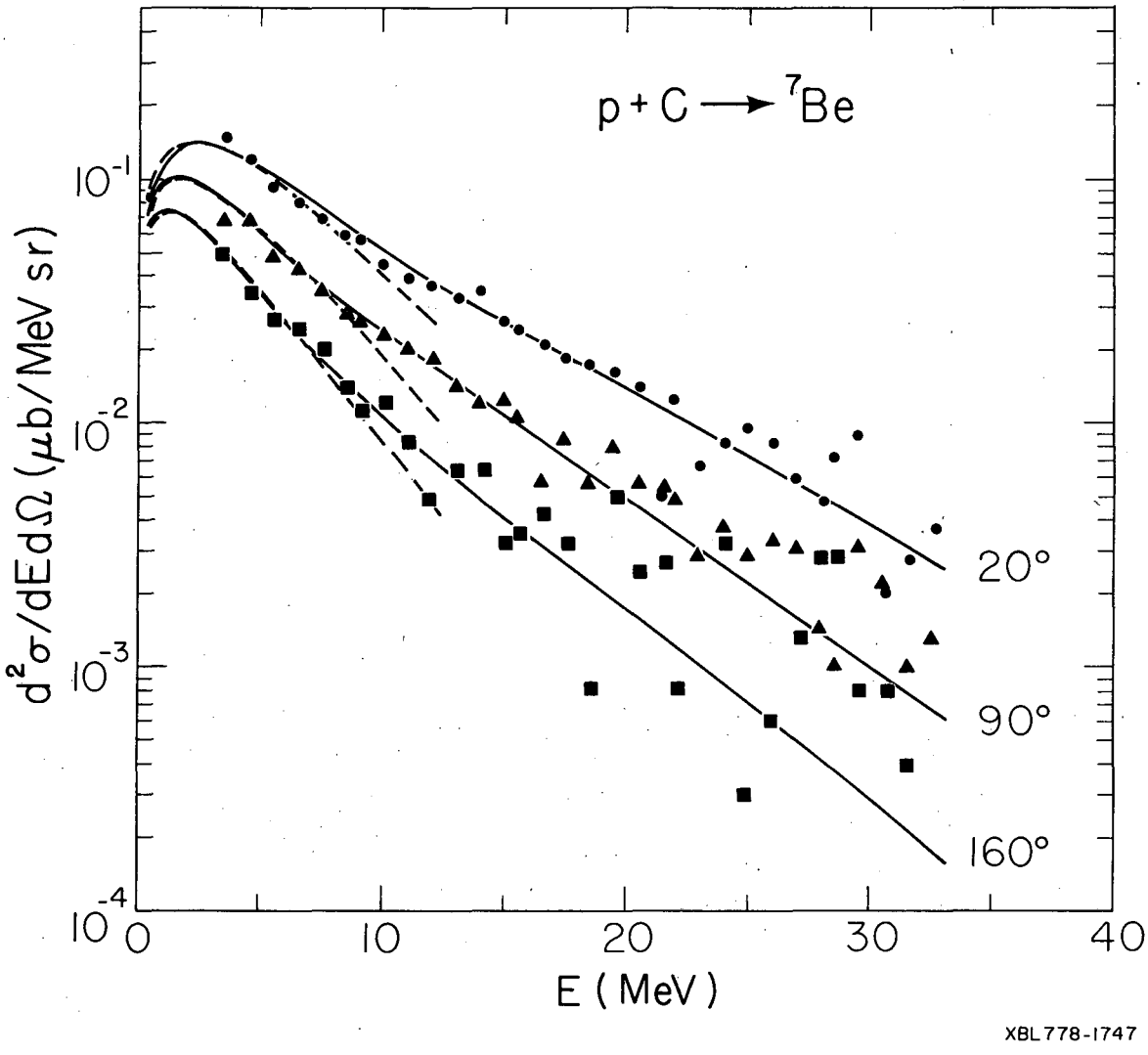
p + C → ⁷Be
d²σ/dEdΩ (μb/MeV sr)
10⁻¹
10⁻²
10⁻³
10⁻⁴
0
10
20
30
40
E (MeV)
20°
90°
160°
XBL778-1747

Fig. 3

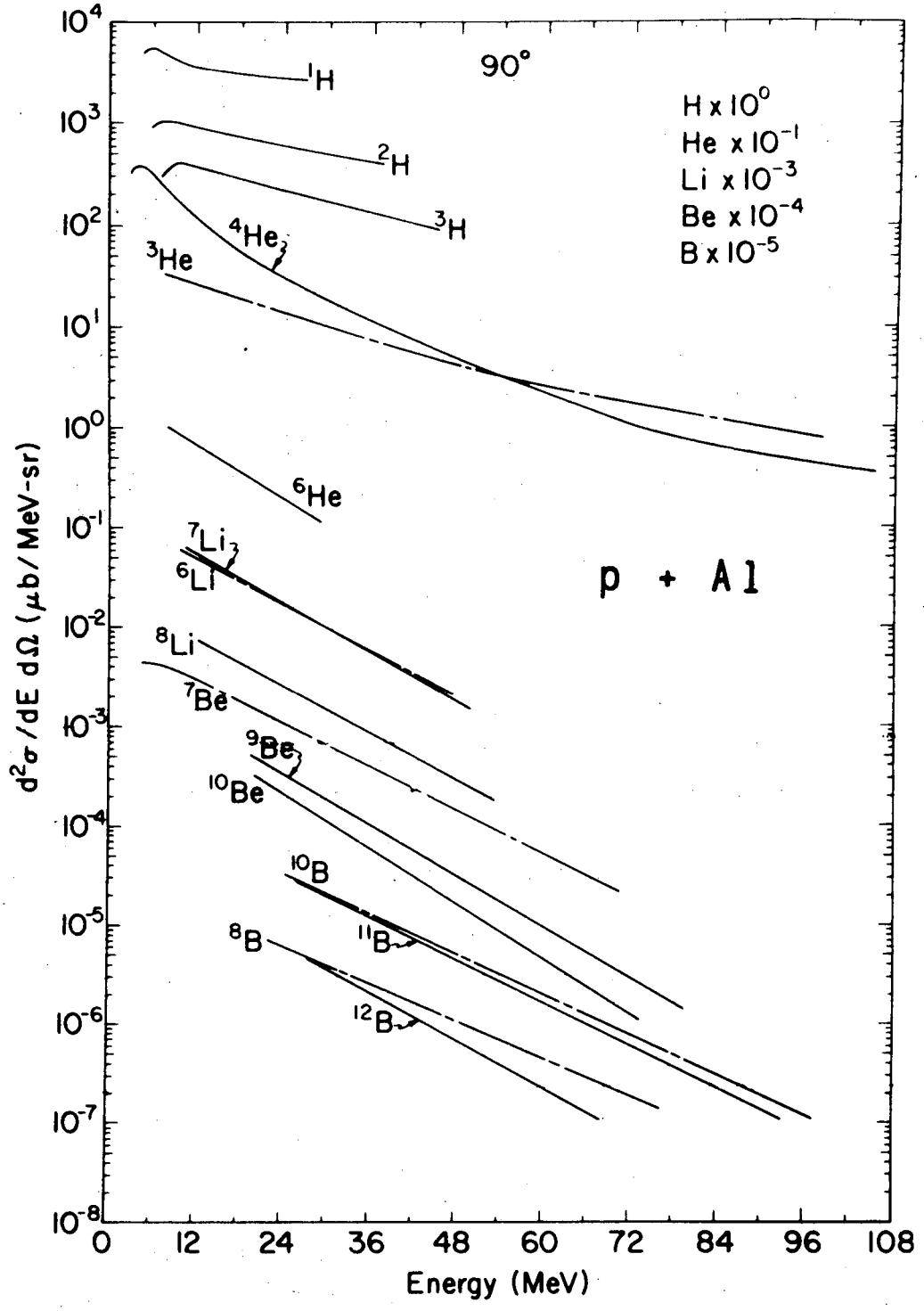

XBL705-2835

Fig. 4

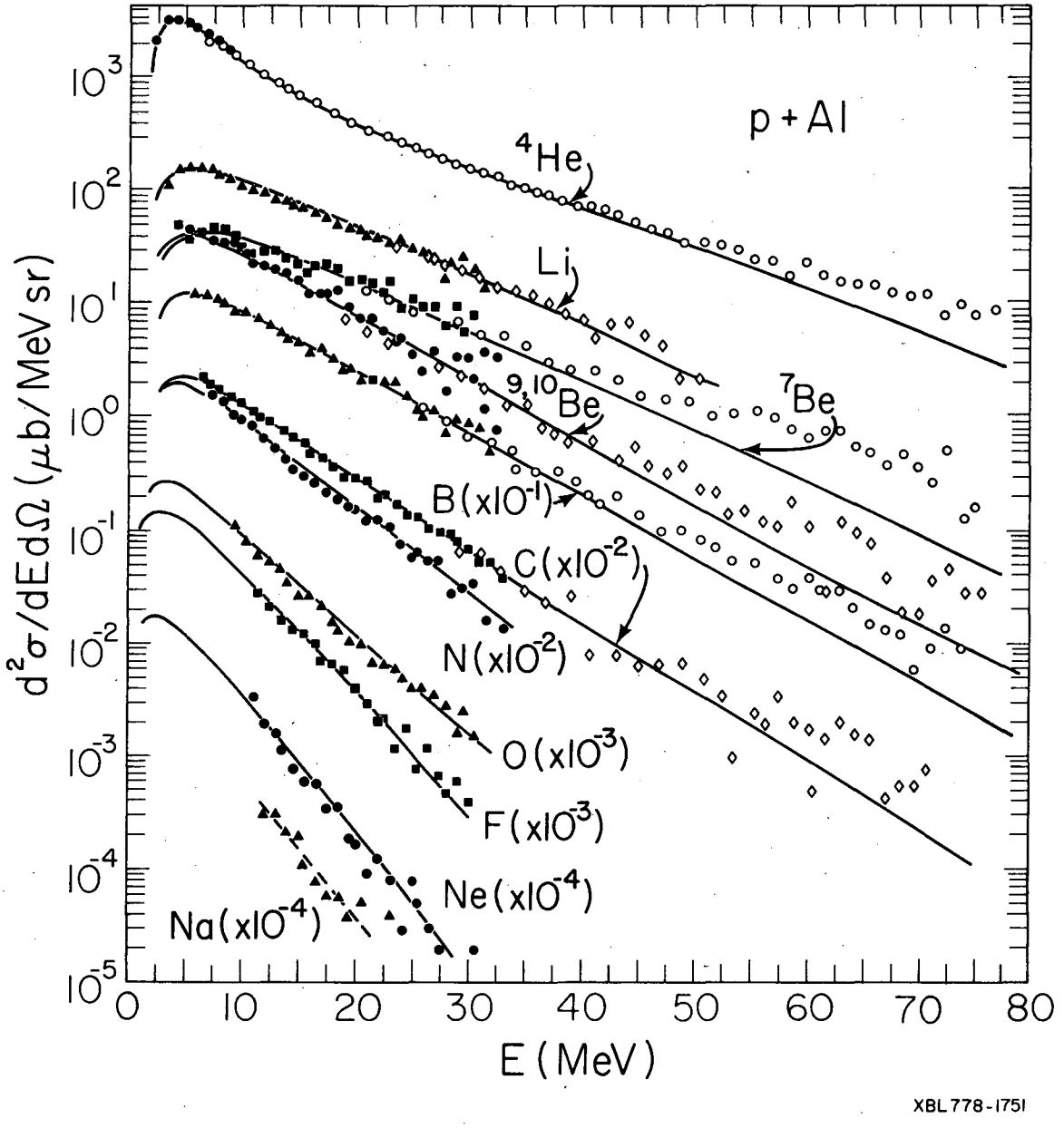
p + Al
^{4}He
Li
^{9,10}Be
^{7}Be
B(x10^{-1})
C(x10^{-2})
N(x10^{-2})
O(x10^{-3})
F(x10^{-3})
Ne(x10^{-4})
Na(x10^{-4})
$d^2\sigma/dE\,d\Omega$ (μb/MeV sr)
E (MeV)
XBL778-1751

Fig. 5

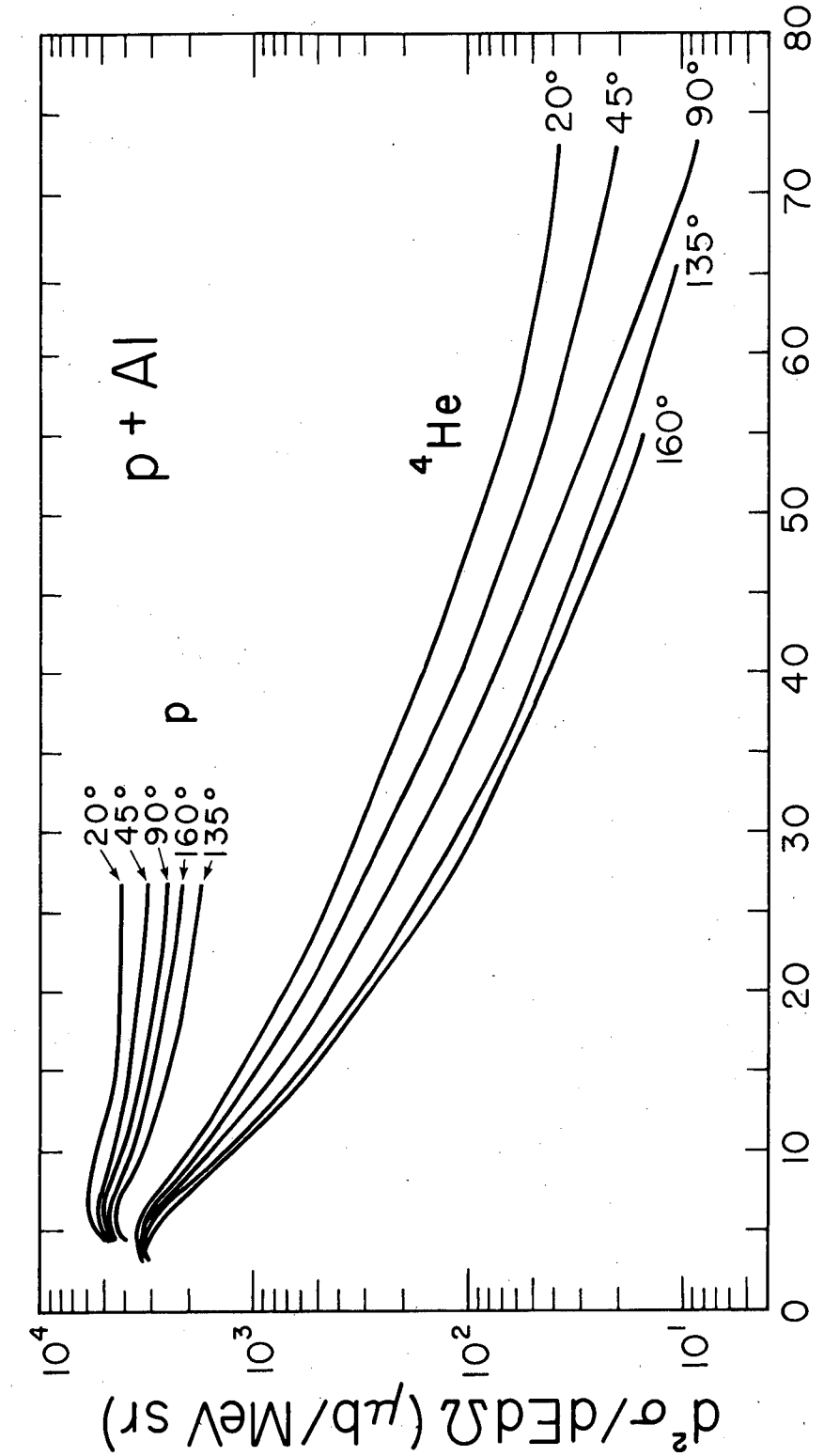

XBL 778-1745

Fig. 6

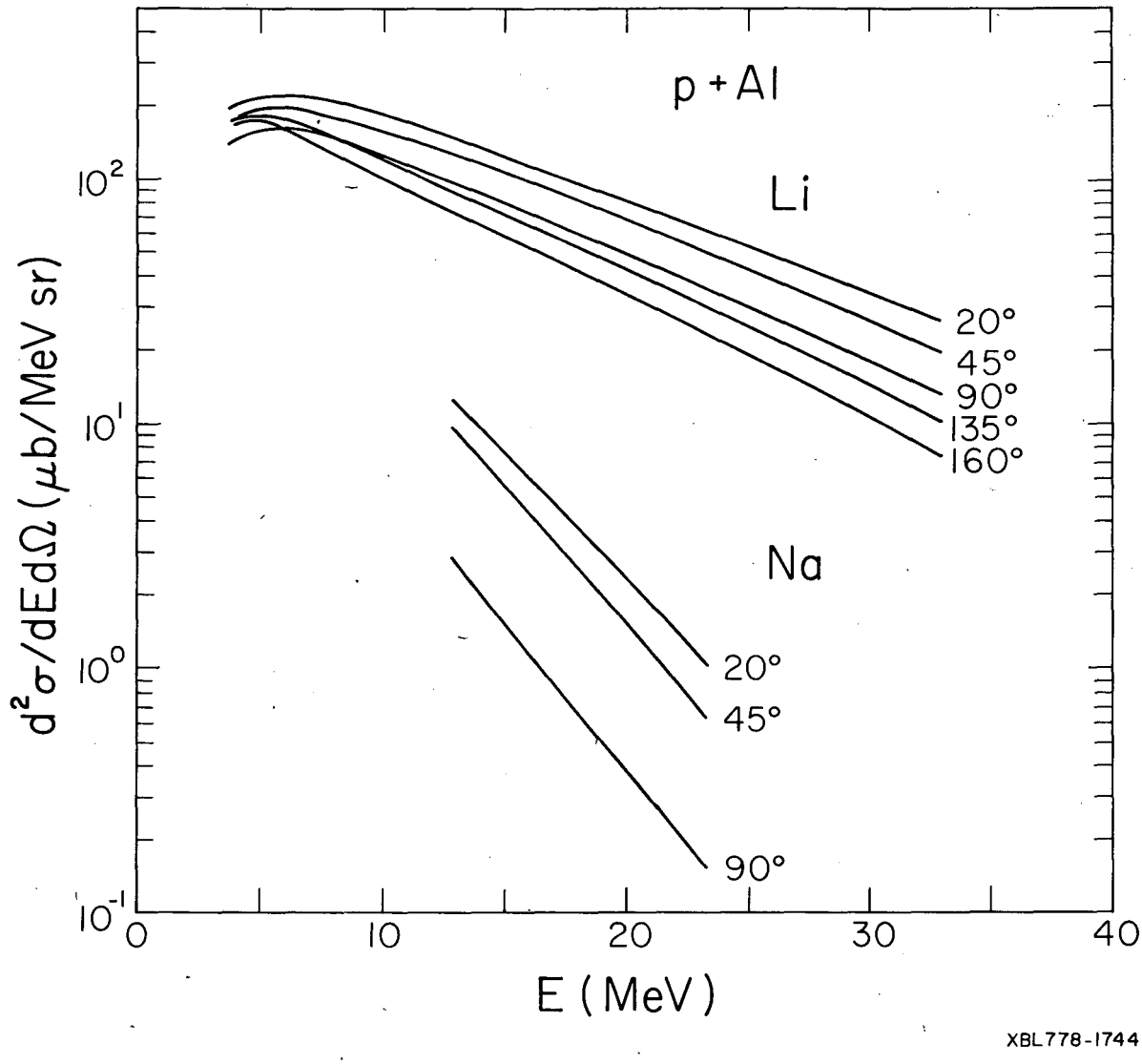
p + Al
Li
20°
45°
90°
135°
160°
Na
20°
45°
90°
$d^2\sigma/dEd\Omega$ (μb/MeV sr)
10^2
10^1
10^0
10^{-1}
0
10
20
30
40
E (MeV)
XBL778-1744

Fig. 7

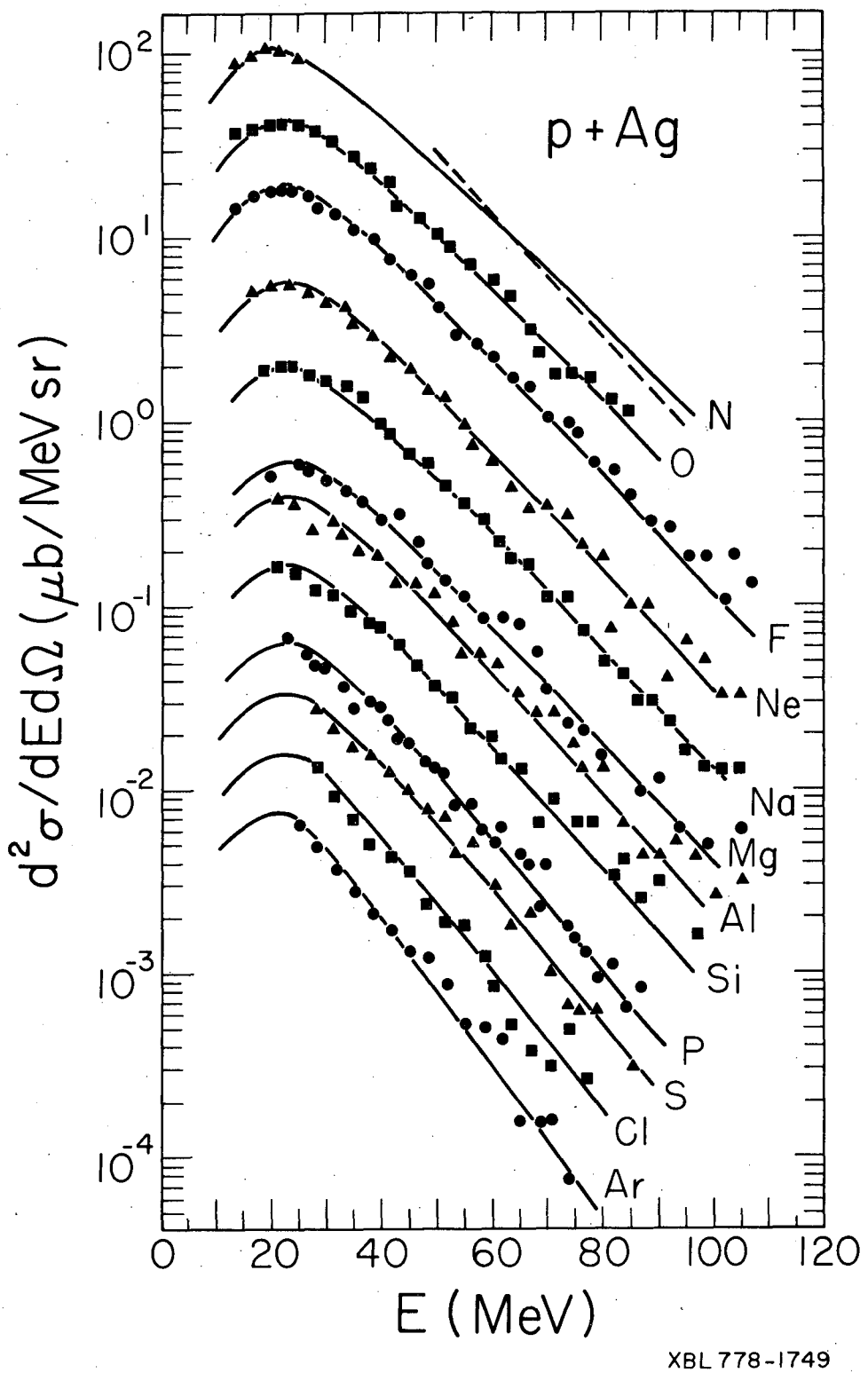

Fig. 8

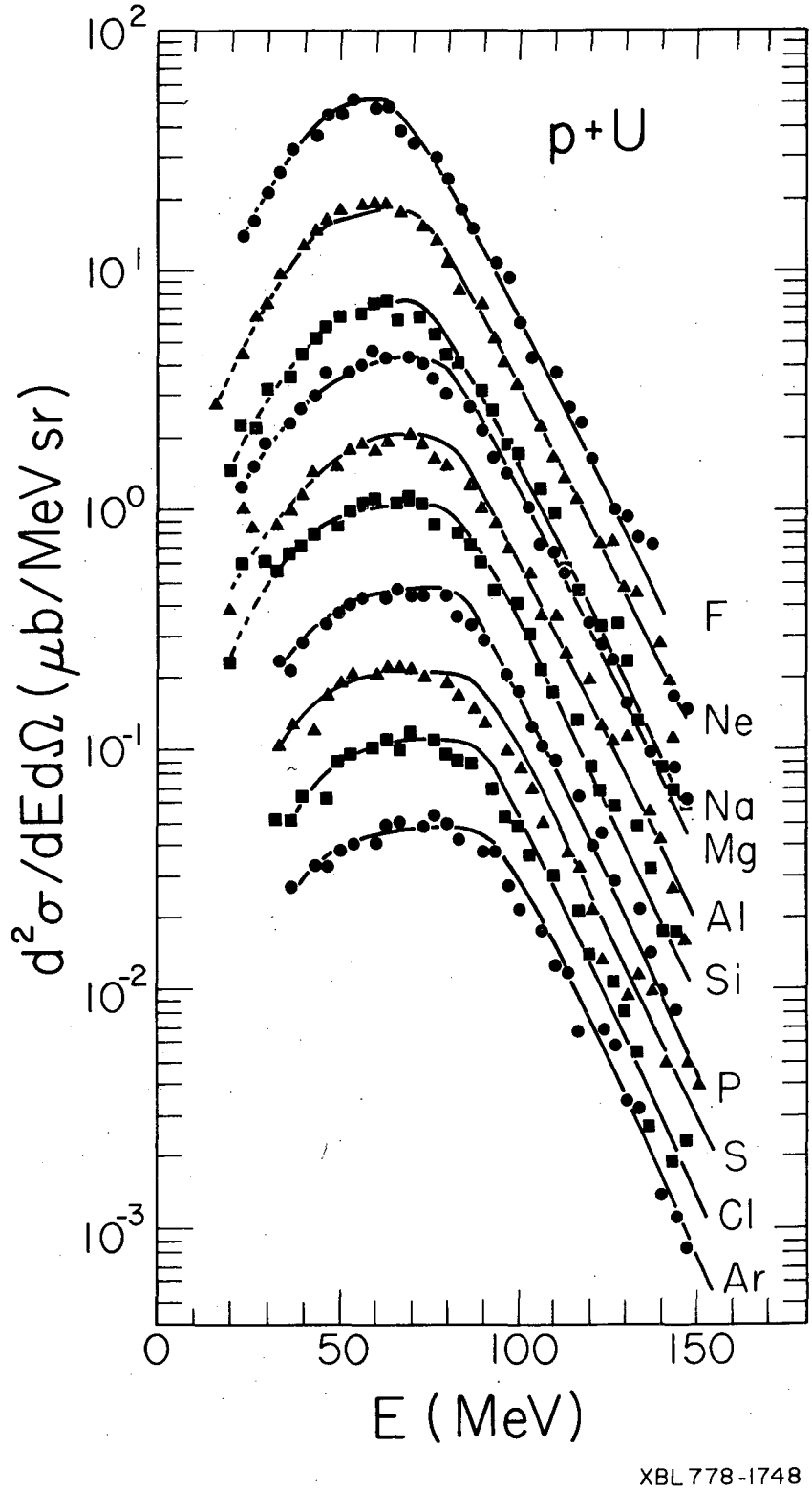
p+U
F
Ne
Na
Mg
Al
Si
P
S
Cl
Ar
$d^2\sigma/dEd\Omega$ (μb/MeV sr)
E (MeV)
10^2
10^1
10^0
10^{-1}
10^{-2}
10^{-3}
0
50
100
150
XBL 778-1748

Fig. 9

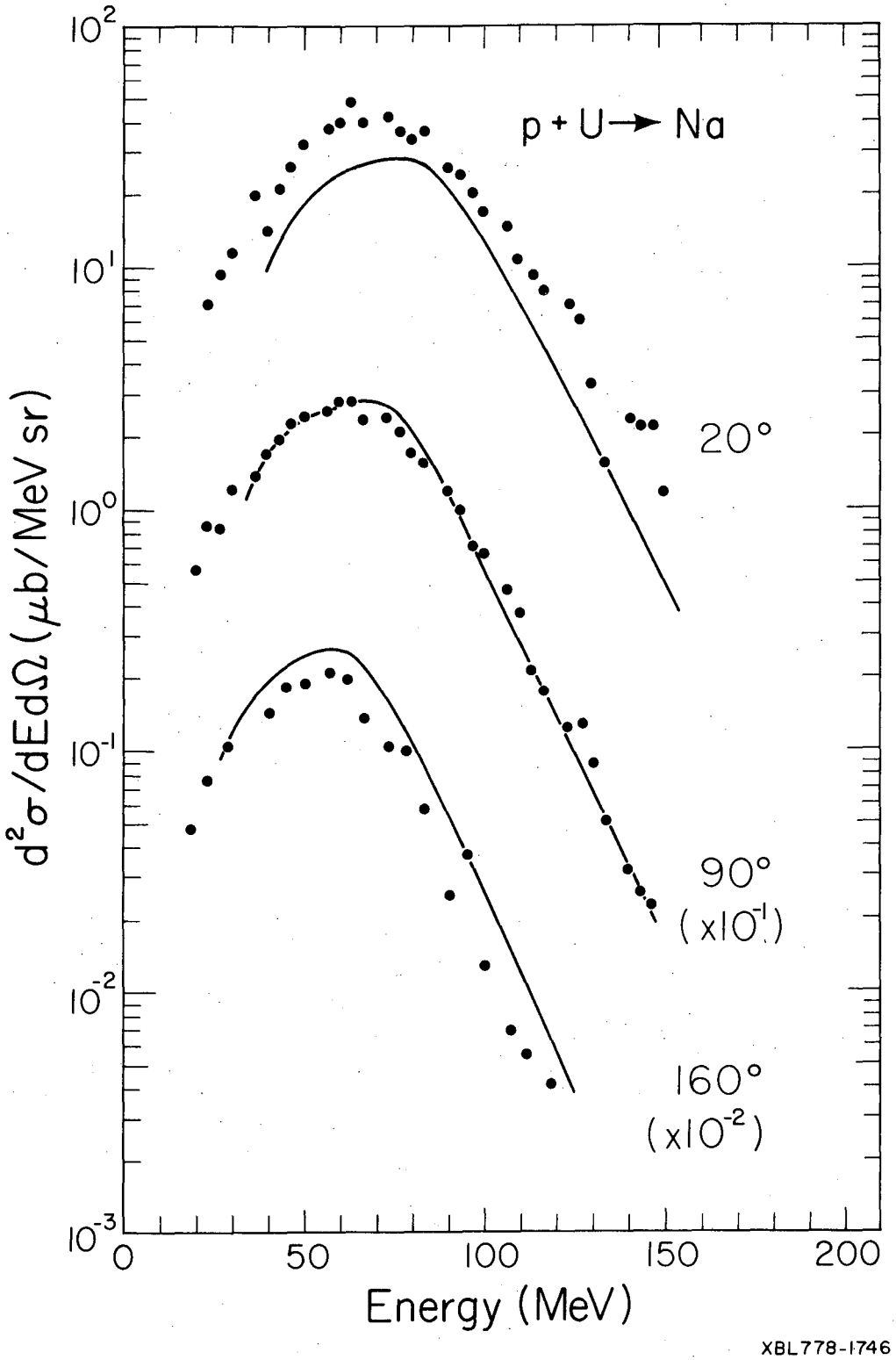
p + U → Na
20°
90°
(x10⁻¹)
160°
(x10⁻²)
d²σ/dEdΩ (μb/MeV sr)
Energy (MeV)
10²
10¹
10⁰
10⁻¹
10⁻²
10⁻³
0
50
100
150
200
XBL778-1746

Fig. 10

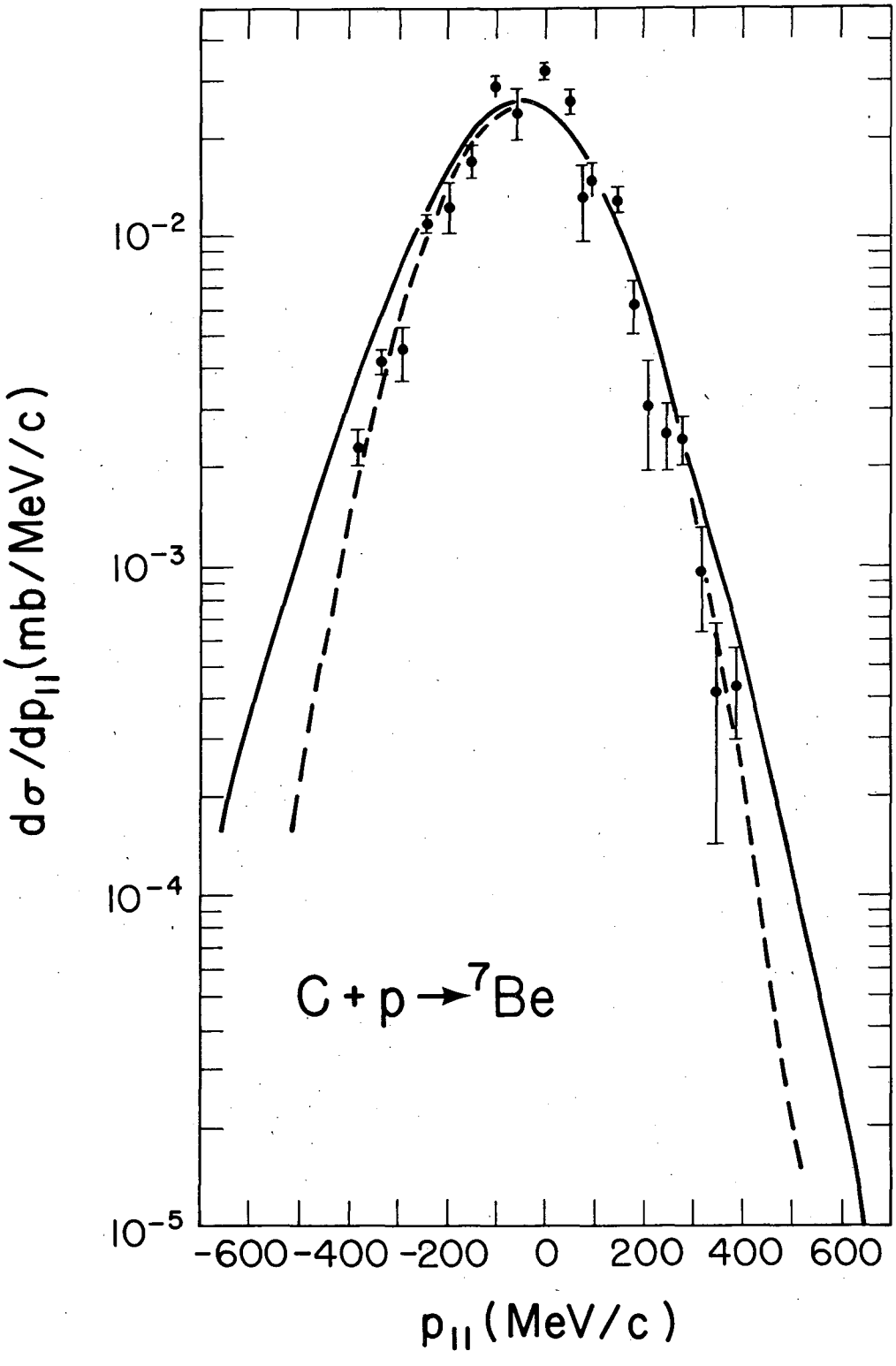
$d\sigma/dp_{11}$(mb/MeV/c)
10^{-2}
10^{-3}
10^{-4}
10^{-5}
C + p → ^{7}Be
-600 -400 -200 0 200 400 600
p_{11} (MeV/c)
XBL 778-1743

Fig. 11

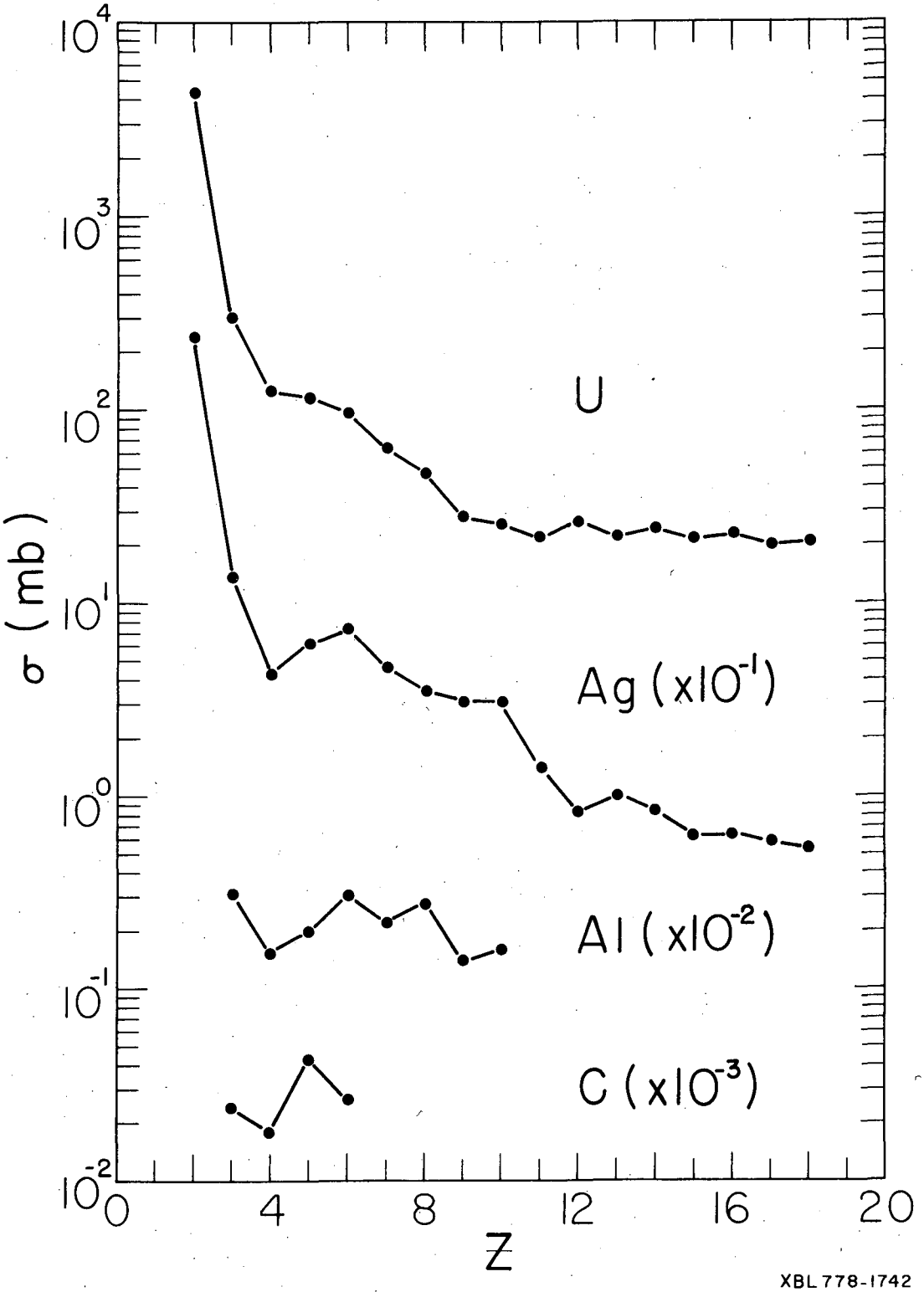
10^4
10^3
10^2
10^1
10^0
10^{-1}
10^{-2}
σ (mb)
U
Ag (x10^{-1})
Al (x10^{-2})
C (x10^{-3})
0
4
8
12
16
20
Z
XBL 778-1742

Fig. 12

TECHNICAL INFORMATION DEPARTMENT
LAWRENCE BERKELEY LABORATORY
UNIVERSITY OF CALIFORNIA
BERKELEY, CALIFORNIA 94720